ORIGINAL ARTICLE

Cancer Science WILEY

Tumor cell–released LC3-positive EVs promote lung metastasis of breast cancer through enhancing premetastatic niche formation

Xiaotong Sun[1] | Xuru Wang[1] | Chunguang Yan[1] | Shiya Zheng[2] | Rong Gao[1] | Fang Huang[1] | Yiting Wei[1] | Zhifa Wen[1] | Yongqiang Chen[1] | Xiaohe Zhou[1] | Xueming Liu[1] | Bohao Chen[1] | Yuqing Shen[1] | Yunlang Cai[3] | Ning Pan[1] | Lixin Wang[1]

[1]Jiangsu Provincial Key Laboratory of Critical Care Medicine, Department of Immunology, Medical School of Southeast University, Nanjing, China

[2]Department of Oncology, Zhongda Hospital, Medical School of Southeast University, Nanjing, China

[3]Department of Obstetrics and Gynecology, Zhongda Hospital, Medical School of Southeast University, Nanjing, China

Correspondence
Lixin Wang and Ning Pan, Jiangsu Provincial Key Laboratory of Critical Care Medicine, Department of Immunology, Medical School of Southeast University, 210009 Nanjing, China.
Emails: lxwang@seu.edu.cn; 101010019@seu.edu.cn

Funding information
National Natural Science Foundation of China, Grant/Award Number: 31370895, 31670918, 31970849 and 81872122

Abstract

Most breast cancer–related deaths are caused by metastasis in vital organs including the lungs. Development of supportive metastatic microenvironments, referred to as premetastatic niches (PMNs), in certain distant organs before arrival of metastatic cells, is critical in metastasis. However, the mechanisms of PMN formation are not fully clear. Here, we demonstrated that chemoattractant C–C motif chemokine ligand 2 (CCL2) could be stimulated by heat shock protein 60 (HSP60) on the surface of murine 4T1 breast cancer cell–released LC3$^+$ extracellular vesicles (LC3$^+$ EVs) via the TLR2-MyD88-NF-κB signal cascade in lung fibroblasts, which subsequently promoted lung PMN formation through recruiting monocytes and suppressing T cell function. Consistently, reduction of LC3$^+$ EV release or HSP60 level or neutralization of CCL2 markedly attenuated PMN formation and lung metastasis. Furthermore, the number of circulating LC3$^+$ EVs and HSP60 level on LC3$^+$ EVs in the plasma of breast cancer patients were positively correlated with disease progression and lung metastasis, which might have potential value as biomarkers of lung metastasis in breast cancer patients (AUC = 0.898, 0.694, respectively). These findings illuminate a novel mechanism of PMN formation and might provide therapeutic targets for anti-metastasis therapy for patients with breast cancer.

KEYWORDS
HSP60, LC3$^+$ EVs, lung fibroblasts, premetastatic niche, secretory autophagosomes

---

---

1 | INTRODUCTION

Breast cancer (BC) is the most common diagnosed malignancy in women worldwide. Despite significant advances in the early detection and treatment of BC, many patients still die from distant organ metastasis.[1] The lung is one of the most common and deadliest sites of BC metastasis, particularly in patients with triple-negative breast cancer (TNBC).[2] Lung metastasis remains difficult to treat; 60%-70% of patients die of BC due to lung metastasis.[3]

The colonization of circulating tumor cells (CTCs) in the distant organs is a key initial step of metastasis.[4,5] The formation of supportive metastatic environments in distant organs, termed the premetastatic niche (PMN), is essential for CTC colonization, seeding, and survival.[6,7] Owing the critical role in distal organ metastasis, numerous efforts are made to reduce PMN formation in order to improve the outcome of malignancy. It has been reported that tumor-secreted factors (TDSFs) such as vascular endothelial growth factor (VEGF),[8] tumor necrosis factor (TNF)-α,[9] osteopontin,[10] stromal cell–derived factor[11] and nicotinamide phosphoribosyl transferase (NAMPT)[12] could all influence PMN formation through different mechanisms. For example, tumor-derived extracellular vesicles (EVs), such as exosome, could travel far from their original site to act as the potential mediators of PMN.[13,14] However, it is still uncertain whether other TDSFs sited in the primary tumor could also contribute to the formation of PMN and the fortune of malignancy could be affected or not by modulating these TDSFs.

Recently, secretory autophagosomes, a new type of LC3+ EVs, have received widespread attention in exploring various disease features. Loss of lysozyme released by intestinal Paneth cells is related to increased risk of Crohn's disease.[15] Moreover, cardiomyocyte-released autophagosomes containing defective mitochondria phagocyted by macrophages are capable of improving cardiomyocyte health.[16] Our previous studies have shown that tumor cell–released LC3+ EVs (termed as tumor cell–released autophagosomes [TRAPs]) isolated from murine tumor cell lines and pleural effusions or ascites of cancer patients were distinct from exosomes.[17-20] LC3+ EVs could modulate the immunosuppressive activities of B cells,[17] neutrophils,[18] macrophages,[19] and CD4+ T cells[20] in tumor microenvironment. However, it is unclear whether these LC3+ EVs could modulate PMN formation in distant organs and affect metastasis.

2 | MATERIALS AND METHODS

2.1 | Patients

Details are described in Appendix S1.

2.2 | Mice, cell culture, and reagents

Details are described in Appendix S1.

2.3 | LC3+ EVs isolation and characterization

LC3+ EVs were collected from tumor cells as previously described.[21] Briefly, cell supernatants were collected and centrifuged at 450 g for 10 minutes to exclude dead cells and debris. The supernatant was further centrifuged at 12,000 g for 30 minutes to harvest LC3+ EVs–containing pellet. Subsequently, EVs were washed twice with PBS containing NH4Cl plus EDTA. The LC3+ EVs–containing pellet was washed with PBS and isolated with magnetic beads (Miltenyi Biotec) combined with LC3B antibody (Cell Signaling Technology). The purity of LC3+ EVs was determined by flow cytometry (FCM), Western blot, and TEM.

2.4 | LC3+ EVs stimulation and labeling

Details are described in Appendix S1.

2.5 | Determination of circulating LC3+ EV absolute number

The fresh blood was centrifuged for 10 minutes at 1000 g and plasma was collected. After centrifugation for 10 minutes at 3000 g, 100 μl of plasma was stained with anti-LC3B antibody for 30 minutes and washed with PBS for 20 minutes at 12,000 g, and then 10,000 events of counting beads were added in each tube. FCM acquisition stopped after 5000 events had been counted in the counting beads gate, and the number of LC3+ EVs in 100 μl of plasma was calculated.

2.6 | Lung fibroblast isolation

Details are described in Appendix S1.

2.7 | Quantitative real-time PCR and RNA-sequencing analysis

Details are described in Appendix S1.

2.8 | Flow cytometry

The single-cell suspension was blocked with mouse FcR blocking (Miltenyi Biotec) prior to surface staining. Fixable viability dye eFluor 520 (eBioscience) was used to exclude dead cells. For intracellular staining in T cells, after ex vivo stimulation with the leukocyte activation cocktail (BD Biosciences) for 5 hours, cells were fixed and permeabilized by using a fixation/permeabilization kit (BD Biosciences) followed by intracellular cellular staining after staining with surface antibodies. Data were acquired on BD FACS Calibur and analyzed by Flow-Jo.

2.9 | Western blot analysis

Details are described in Appendix S1.

2.10 | ELISA

Details are described in Appendix S1.

2.11 | Lung leakage experiments

Details are described in Appendix S1.

2.12 | Chemotaxis assays

Details are described in Appendix S1.

2.13 | CCL2 inhibition in vivo

Two days following tumor inoculation, mice were injected intraperitoneally with anti-CCL2 antibody (10 mg /kg/mouse) (clone 2H5; BioXCell). Injections were performed every 2 days to a total of four injections.

2.14 | Animal models

For defining the premetastatic lungs, luc$^+$-4T1 cells were subcutaneously injected into the right fourth mammary fat pads of mice, and lungs were harvested for the luciferase detection. The period without luc$^+$-4T1 cells was defined as premetastatic phase.

To assess the PMN formation, *Becn1* KD-4T1 or *Hsp60* KD-4T1 cells (5×10^5 cells/mouse/100 µl) were subcutaneously injected into the right fourth mammary fat pads of mice. The plasma was collected for LC3$^+$ EV number counting and HSP60 detection. On day 10, the frequencies of monocytes (Mo), macrophages, T cells, IFN-γ$^+$ T cells, and PD-L1 expression were evaluated in the lung. Lung leakage was evaluated by immunofluorescence. In the LC3$^+$ EV–educated model, LC3$^+$ EVs (10 µg) were injected intravenously every other day for a total of five treatments. On day 10, the frequencies of Mo, macrophages, T cells, IFN-γ$^+$ T cells, PD-L1 expression, and lung leakage were evaluated by FCM.

To evaluate the lung metastasis, *Becn1* KD-4T1 or *Hsp60* KD-4T1 cells (5×10^5 cells/mouse/100 µl) were subcutaneously injected into the right fourth mammary fat pads of mice. On day 35, mice were euthanized, and their lungs were collected. In the LC3$^+$ EV–educated model, LC3$^+$ EVs (10 µg) were injected intravenously every other day for a total of five treatments, followed by intravenous injection of 4T1 cells (1×10^5 cells). Mice were sacrificed 21 days later, and their lungs were fixed with Bouin's solution.

2.15 | Statistical analysis

Statistical analyses were performed using SPSS23.0 and GraphPad Prism 8.0. Experimental data came from three independent experiments. The two-tailed unpaired Student's test was applied to compare two normally distributed parameters, and the Mann-Whitney U-test was applied to compare the non-normally distributed parameters between two groups. Multiple groups were compared with one-way ANOVA and Bonferroni post hoc test for data that fulfilled normal distribution, and the Kruskal-Wallis test was used for not normally distributed data. Binary logistic regression analysis was used to identify independent risk factors. Receiver-operating characteristic (ROC) curves were constructed and area under the curve (AUC) values calculated to estimate the accuracy of variables for prediction of lung metastasis. All data are presented as the mean value ± SEM and $p < 0.05$ was considered significant (*$p < 0.05$; **$p < 0.01$; ***$p < 0.001$; ****$p < 0.0001$; NS, not significant).

3 | RESULTS

3.1 | Primary tumor cell–derived circulating LC3$^+$ EVs promote lung PMN formation

To investigate the role of primary tumor cell–released LC3$^+$ EVs in the process of lung metastasis, a *Becn1* knockdown 4T1 cells (*Becn1* KD-4T1) tumor–bearing model was established (Figure 1A). *Becn1* knockdown in 4T1 cells diminished intracellular LC3-II accumulation and markedly reduced LC3$^+$ EVs secretion but had no effect on exosome secretion (Figure S1A,B). In vitro proliferation of *Becn1* KD-4T1 cells has no significant change compared with *Becn1* NC-4T1 cells (Figure S1C). Although the overall tumor growth was delayed in *Becn1* KD-4T1–bearing mice, the tumor size of *Becn1* KD-4T1–bearing mice and that of *Becn1* NC-4T1–bearing mice were comparable within 14 days (Figure S1D). Western blot analysis confirmed the downregulation of Beclin1 in *Becn1* KD-4T1 tumor tissues (Figure S1E). Notably, cLC3$^+$ EVs of *Becn1* KD-4T1–bearing mice were significantly reduced compared with those of *Becn1* NC-4T1–bearing mice (Figure S1F, Figure 1B). More importantly, significant reduction of spontaneous lung metastasis in *Becn1* KD-4T1–bearing mice was observed compared with that in *Becn1* NC-4T1–bearing mice (Figure S2A, Figure 1C), suggesting a promoting role of cLC3$^+$ EVs in the process of lung metastasis.

Premetastatic niches formation plays a vital role in the process of metastasis.[4,7] We thus investigated the effect of LC3$^+$ EVs in the lung PMN formation. To define the premetastatic lung, luciferase-labeled 4T1 cells (luc$^+$ 4T1) tumor–bearing mice model was established (Figure 1A). No luciferase could be detected in the lung within 14 days, indicating this period is the premetastatic phase (Figure 1D). The recruitment of bone marrow–derived cells (BMDCs) to metastatic sites has been reported to be one of the major hallmarks of PMN formation.[22,23] Significant accumulation of CD11b$^+$ Ly6C^{high} Mo in the lung were observed on day 7, 10, and 14 after subcutaneous
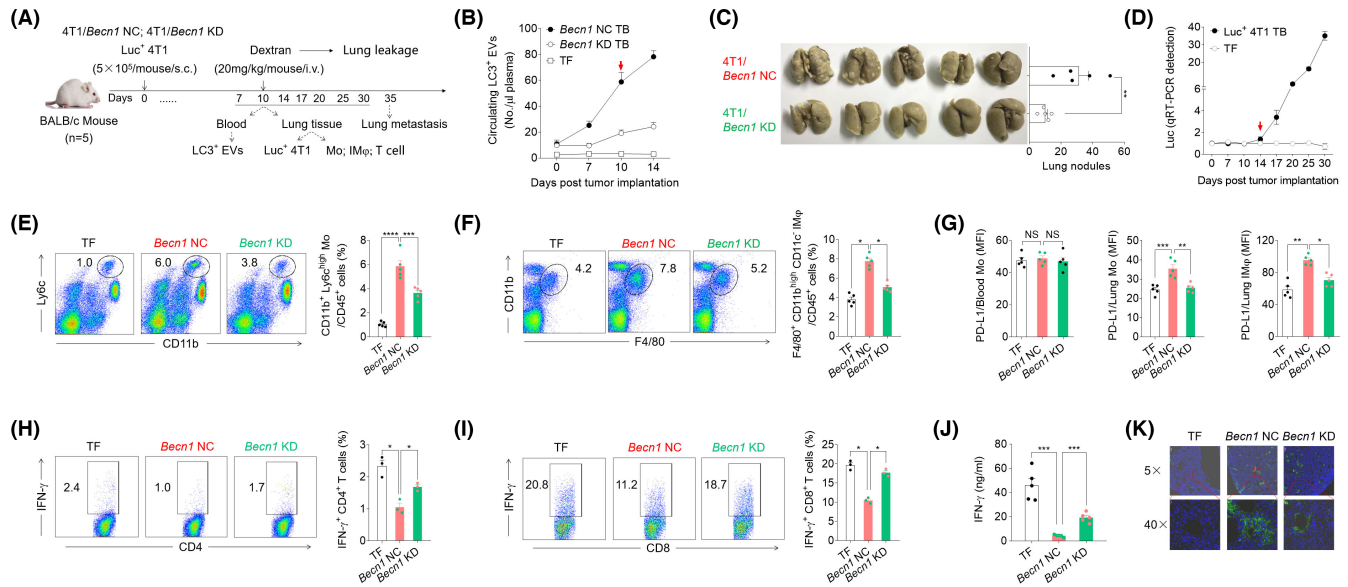
FIGURE 1 Primary tumor–derived circulating LC3$^+$ extracellular vesicles (EVs) mediate premetastatic niche (PMN) formation and promote lung metastasis. (A), Schema for detection of PMN formation and lung metastasis in the indicated 4T1-bearing mice. (B), Peripheral blood from indicated mice was collected for counting the number of cLC3$^+$ EVs by flow cytometry (FCM). (C), BALB/c mice ($n = 5$) were s.c. injected with *Becn1* NC- or *Becn1* KD-4T1 cells, and the lung metastatic nodules were counted 35 d later. (D), The lungs were harvested from luc$^+$-4T1 TB and tumor-free (TF) mice for detecting luciferase by qPCR. E-K, BALB/c mice ($n = 5$) were injected subcutaneously with *Becn1* NC- or *Becn1* KD-4T1 cells. On day 10, the proportion of monocytes (Mo) (E) and interstitial macrophages (IMφ) (F) in the lung, and PD-L1 expression on Mo and IMφ was detected by FCM (G). Intracellular IFN-γ expression of CD4$^+$ (H) or CD8$^+$ T cells (I) was analyzed by FCM, and IFN-γ secretion in supernatants was detected by ELISA (J). Immunofluorescence images of lung vascular leakage (K). Data were expressed as means ± SEM.
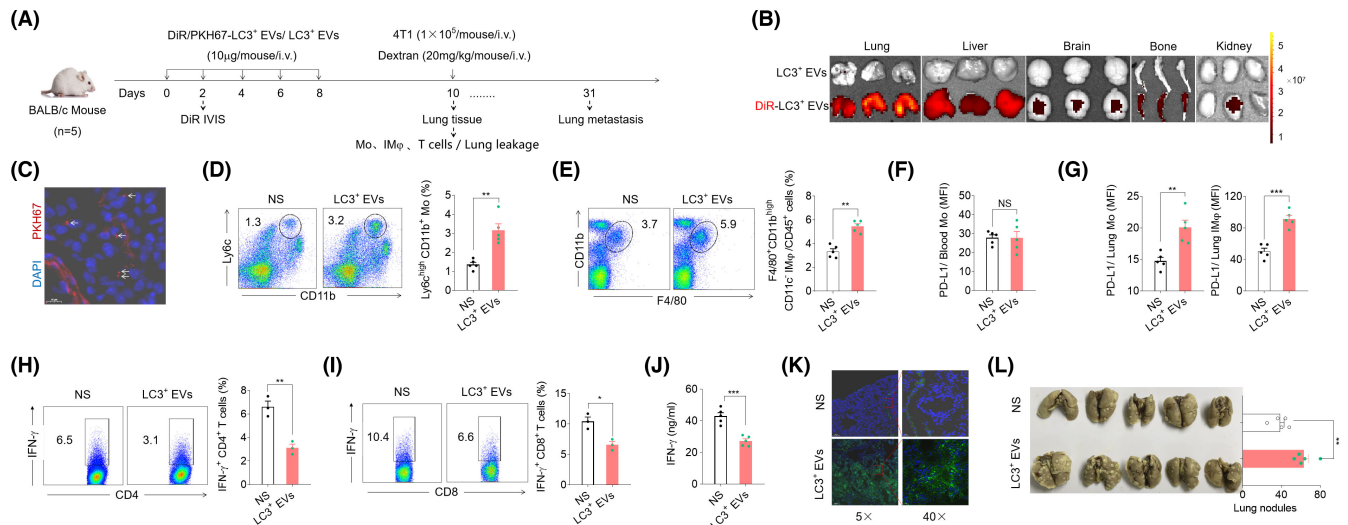

FIGURE 2 Circulating LC3$^+$ extracellular vesicles (EVs) promote lung premetastatic niche (PMN) formation. (A), Schema for detection of PMN formation and lung metastasis in LC3$^+$ EVs–educated mice. (B), DiR-labeled LC3$^+$ EVs distribution in the lungs and other organs detected by IVIS. (C), PKH67-labeled LC3$^+$ EVs distribution in the lungs detected by fluorescence microscope (scale bar, 10 μm). D-K, BALB/c mice ($n = 5$) were i.v. injected with 4T1-LC3$^+$ EVs every other day for five times. The proportion of lung monocytes (Mo) (D) and interstitial macrophages (IMφ) E, PD-L1 expression on Mo in blood (F) and lung, and IMφ in lung were detected by flow cytometry (FCM) (G). Intracellular IFN-γ expression of CD4$^+$ (H) or CD8$^+$ T cells (I) was analyzed by FCM, and IFN-γ secretion in supernatants was detected by ELISA (J). Immunofluorescence images of lung vascular leakage (K). (L) BALB/c mice ($n = 5$) were i.v. injected with 4T1-LC3$^+$ EVs every other day for five times followed by 4T1 cells i.v. injection. 21 d later, lung metastatic nodules were assessed. Data were expressed as means ± SEM.

implantation of 4T1 cells (Figure S2B). On day 10, the frequency of Mo (Figure 1E) and F4/80$^+$ CD11b^{hi} CD11c$^-$ interstitial macrophages (IMφ) (Figure 1F) and their surface PD-L1 expression (Figure 1G)

in the lung of *Becn1* NC-4T1 tumor–bearing mice was significantly increased compared with tumor-free (TF) mice. Interestingly, compared with *Becn1* NC-4T1–bearing mice, the frequency of Mo and

IMφ and their PD-L1 expression in *Becn1* KD-4T1–bearing mice were dramatically decreased (Figure 1E–G), while PD-L1 expression on Mo in peripheral blood remained the same (Figure 1E–G). Meanwhile, IFN-γ⁺ CD4⁺ T cells, IFN-γ⁺ CD8⁺ T cells, and total IFN-γ secretion in lung tissues from tumor-bearing mice were significantly decreased compared with TF mice in vitro, while the proportion of CD4⁺ T cells and CD8⁺ T cells did not change significantly (Figure S2C,D). Compared with *Becn1* NC-4T1–bearing mice, the frequencies of IFN-γ⁺ CD4⁺ T cells and IFN-γ⁺ CD8⁺ T cells and total IFN-γ secretion were partially recovered in *Becn1* KD-4T1–bearing mice (Figure 1H–J). Moreover, enhanced vascular permeability in the lung of *Becn1* NC-4T1–bearing mice was observed compared with TF mice, while the vascular permeability in the lung of *Becn1* KD-4T1–bearing mice was decreased (Figure 1K). Collectively, these results show that on day 10 after tumor cell subcutaneous injection, lung PMN infiltrated with Mo and macrophages, enhanced lung permeability, and suppressed T cell function have been formed. More importantly, the PMN in the lung is diminished in *Becn1* KD-4T1–bearing mice, suggesting an enhancing role of cLC3⁺ EVs in the lung PMN formation.

To further demonstrate the role of LC3⁺ EVs in lung PMN formation, 4T1 cell–derived LC3⁺ EVs (4T1-LC3⁺ EVs) (Figure S3A–C) labeled with DiR or PKH67 were injected into mice by tail vein (Figure 2A). These LC3⁺ EVs were found to mainly distribute in the lung, and also in liver, brain, and bone (Figure 2B,C). Compared with the normal saline (NS) group, the proportion of lung-infiltrating Mo and IMφ and their PD-L1 levels were dramatically elevated in LC3⁺ Evs–pretreated mice (Figure 2D-G). A lower frequency of IFN-γ⁺ T cells and decreased IFN-γ secretion were observed in LC3⁺ EVs-pretreated mice (Figure 2H-J). Enhanced vascular permeability in the lung was observed in the LC3⁺ EVs–pretreated mice (Figure 2K). Most importantly, pretreatment of mice with LC3⁺ EVs increased lung metastatic colonization (Figure 2L). Taken together, these results further demonstrated that LC3⁺ EVs could induce a proinflammatory and immune-suppressed PMN formation and pave the way for lung metastasis.

3.2 | LC3⁺ EVs enhance CCL2 production in lung fibroblasts via the TLR2-MyD88-NF-kB pathway

To investigate the underlying mechanism through which LC3⁺ EVs promote lung PMN formation, the uptake of 4T1-LC3⁺ EVs in the lung was analyzed by FCM. The results showed that LC3⁺ EVs were mainly taken up by macrophages (46.8%) and fibroblasts (33.0%), respectively (Figure 3A,B).

Fibroblasts have been proved to be involved in the progression of PMN and metastasis.[24] Proinflammatory activation of fibroblasts was previously shown to be functionally important for recruitment of immune cells into the tumor microenvironment.[25,26] As further reinforcement, the primary lung fibroblasts (Figure S4A) were incubated with PKH67-labeled LC3⁺ EVs. Confocal imaging and FCM analysis showed a cytoplasmic localization of PKH67-labeled

LC3⁺ EVs in lung fibroblasts (Figure 3C). Moreover, treatment of lung fibroblasts with LC3⁺ EVs resulted in upregulated expression of αSMA, an activated marker of fibroblasts (Figure S4B). We next aimed to further characterize the LC3⁺ EVs–induced lung fibroblast activation. A total of 666 upregulated genes were found highly enriched in LC3⁺ EVs–stimulated fibroblasts as compared with normal fibroblasts by RNA sequencing. Gene Ontology analysis revealed that differential genes were significantly enriched in inflammatory response (Figure 3D). Among them, CCL2 was the most upregulated abundant gene involved in inflammatory response (Figure 3E, Figure S4C). LC3⁺ EVs induced lung fibroblasts to produce CCL2 in vitro (Figure 3F, Figure S4D). Importantly, ex vivo results showed that CCL2 produced by lung fibroblasts from *Becn1* KD 4T1–bearing mice was significantly decreased compared with that from *Becn1* NC 4T1–bearing mice (Figure 3G). Furthermore, CCL2 produced by lung fibroblasts from 4T1-LC3⁺ EVs–preinjected mice was significantly increased compared with that from mice with NS injection (Figure 3H), indicating that LC3⁺ EVs could induce lung fibroblasts to produce CCL2.

We next explored the mechanism of LC3⁺ EV–mediated CCL2 expression of lung fibroblasts. Pretreatment of lung fibroblasts with an inhibitor of TLR2 or MyD88 attenuated 4T1-LC3⁺ EVs–induced secretion of CCL2 (Figure S4E). Consistently, *Tlr2⁻/⁻* and *Myd88⁻/⁻* mice–derived lung fibroblasts were completely defective in producing CCL2 in response to 4T1-LC3⁺ EVs (Figure 3I). LC3⁺ EVs treatment of lung fibroblasts resulted in the phosphorylation of the NF-ᵏB pathway (Figure 3J), and inhibition of the NF-kB pathway repressed the induction of CCL2 (Figure 3K). These data collectively indicate that 4T1-LC3⁺ EVs could induce CCL2 secretion from lung fibroblasts through the TLR2-MyD88-NF-κB pathway.

3.3 | HSP60 on LC3⁺ EVs promotes lung PMN formation

Next, we identify the molecular components in LC3⁺ EVs that are responsible for stimulating lung fibroblasts to produce CCL2. Pretreatment with proteinase K digestion and sonication impaired the ability of LC3⁺ EVs to stimulate the CCL2 production from lung fibroblasts (Figure 4A), indicating that proteins on the surface of LC3⁺ EVs are involved in the CCL2 induction of fibroblasts. Several ligands of TLR2, including HSP27, HSP60, HSP70, HSP90α, and HMGB1, were detected on the surface of LC3⁺ EVs (Figure S5A). Blocking of HSP60 partially reduced LC3⁺ EVs–induced CCL2 secretion (Figure 4B). Moreover, upon stimulation with LC3⁺ EVs from *Hsp60* KD-4T1 cells, the induction of CCL2 was partially abolished, with a concomitant decline of P65 NF-κB phosphorylation (Figure S5B, Figure 4C,D).

We then evaluated the functional role of HSP60 on LC3⁺ EVs in vivo. Accordingly, compared with *Hsp60* NC 4T1–bearing mice, no significant difference was observed in cLC3⁺ EV number in plasma (Figure S5C), but the HSP60 level on cLC3⁺ EVs from *Hsp60* KD 4T1–bearing mice was markedly decreased (Figure 4F, Figure S5D).
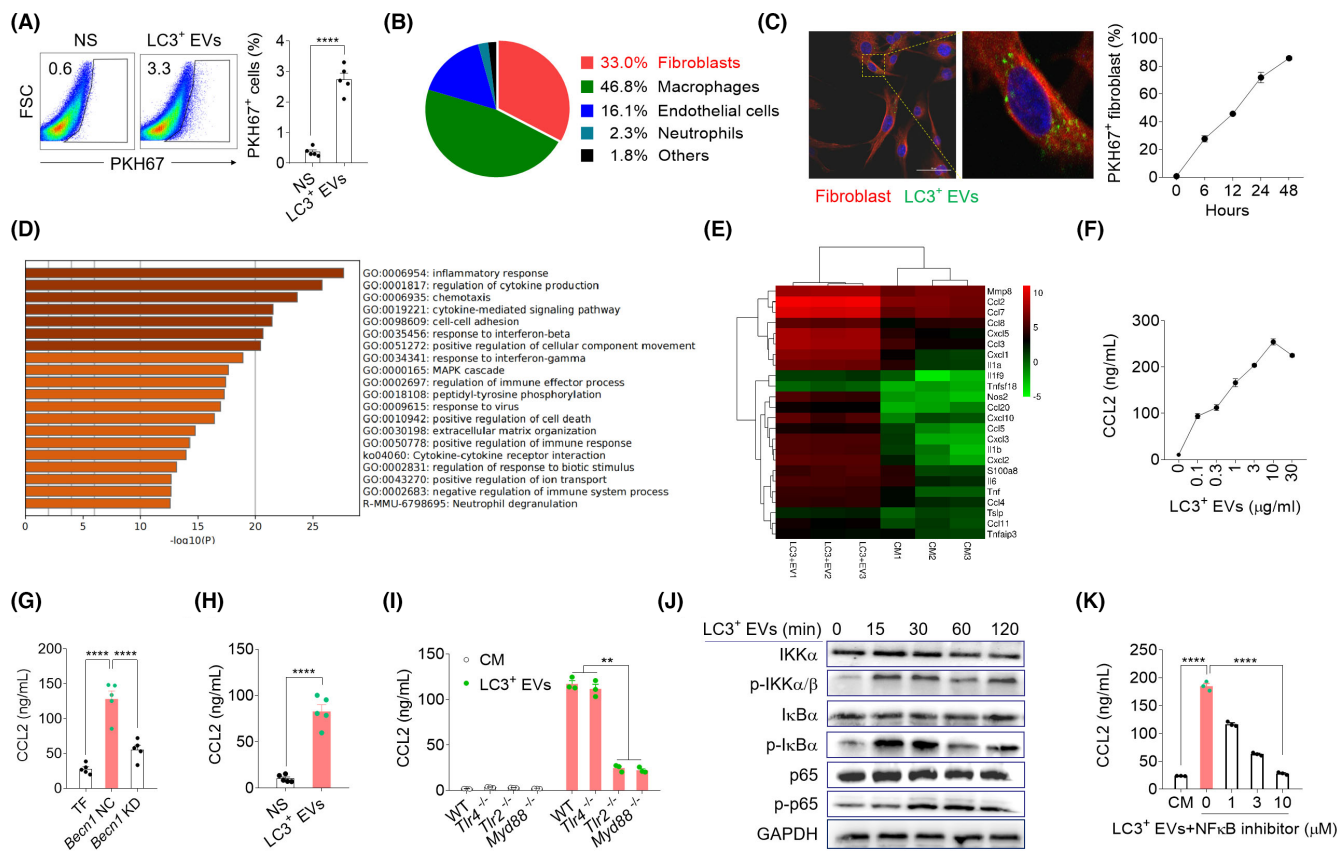
FIGURE 3 LC3$^+$ extracellular vesicles (EVs) activate lung fibroblasts to produce CCL2 via the TLR2-MyD88-NF-kB pathway. (A, B), BALB/c mice ($n = 5$) were i.v. injected with PKH67-labeled LC3$^+$ EVs. PKH67$^+$ cells in the lung (A) and the proportion of indicated cells in PKH67$^+$ cells (B) were analyzed by flow cytometry (FCM). (C), Confocal microscopy images of lung fibroblasts (red) ingesting of PKH67-labeled LC3$^+$ EVs (green) (scale bar, 50 μm). (D), The lung fibroblasts treated with 4T1-LC3$^+$ EVs (10 μg/ml) underwent RNA-sequencing assay, which was followed by functional enrichment analysis of the differentially expressed genes. (E), Heatmap of inflammatory genes that were enriched in an unbiased Gene Ontology (GO) analysis. Analysis was performed on genes significantly upregulated in control versus LC3$^+$ EV–treated lung fibroblasts. (F), ELISA detection of CCL2 secretion by lung fibroblasts incubated with different concentrations of LC3$^+$ EVs for 48 h. G-H, The lung fibroblasts isolated from mice on day 10 after *Becn1* NC- or *Becn1* KD-4T1 cell s.c. injection (G) or after LC3$^+$ EVs i.v. injection (H) were cultured for 48 h. CCL2 levels were determined by ELISA. (I), ELISA detection of CCL2 secretion by lung fibroblasts purified from WT, *Tlr4*$^{-/-}$, *Tlr2*$^{-/-}$, *Myd88*$^{-/-}$ mice incubated with LC3$^+$ EVs for 48 h. (J), Western blot analyses of the phosphorylation of IKKα/β, IκB, p65 in lung fibroblasts treated with LC3$^+$ EVs. (K), The lung fibroblasts were pretreated with NF-κB inhibitor for 1 h and then cocultured with LC3$^+$ EVs for 48 h. CCL2 levels in supernatants were determined by ELISA. Data were expressed as means ± SEM.

Furthermore, a pronounced reduction of CCL2 secretion by lung fibroblasts (Figure 4G) and a substantial decrease in frequency of lung-infiltrating Mo and IMφ were evidenced in *Hsp60* KD 4T1–bearing mice (Figure 4H-I). Moreover, a marked reduction in spontaneous lung metastasis was found in *Hsp60* KD 4T1–bearing mice (Figure 4J). These results suggest that HSP60 bound on the intact LC3$^+$ EVs is the major player responsible for LC3$^+$ EVs–induced lung PMN formation.

3.4 | CCL2 is required for LC3$^+$ EVs–induced inflammatory and immunosuppressive PMN

Monocytes and macrophages infiltration is a known important feature of the premetastatic lung microenvironment,[22,23] and CCL2 is reported as main chemoattractant of Mo snd macrophages. To test the role of CCL2 production of LC3$^+$ EV–stimulated fibroblasts in

macrophage migration, chemotaxis assays were performed by using supernatant from LC3$^+$ EVs–treated fibroblasts. We found that supernatant from LC3$^+$ EVs–treated fibroblasts significantly increased macrophage migration. Moreover, neutralizing CCL2 significantly inhibited LC3$^+$ EVs–stimulated lung fibroblast–induced chemotaxis of macrophages (Figure 5A).

We further validated whether CCL2 is a key player in lung PMN in vivo. CCL2-neutralizing antibody (CCL2 nAb) intraperitoneal injection in tumor-bearing mice suppressed the recruitment of lung-infiltrating Mo and IMφ (Figure 5B,C). The proportion of lung-infiltrating CD4$^+$ T cells and CD8$^+$ T cells did not change significantly (Figure S6A,B). Intriguingly, IFN-γ$^+$ CD4$^+$ T cells, IFN-γ$^+$ CD8$^+$ T cells, and their total IFN-γ secretion were significantly increased post intraperitoneal injection of CCL2 nAb (Figure 5D–F). Importantly, CCL2 blockade inhibited spontaneous lung metastasis of 4T1 tumor–bearing mice (Figure 5G). Above results indicate that
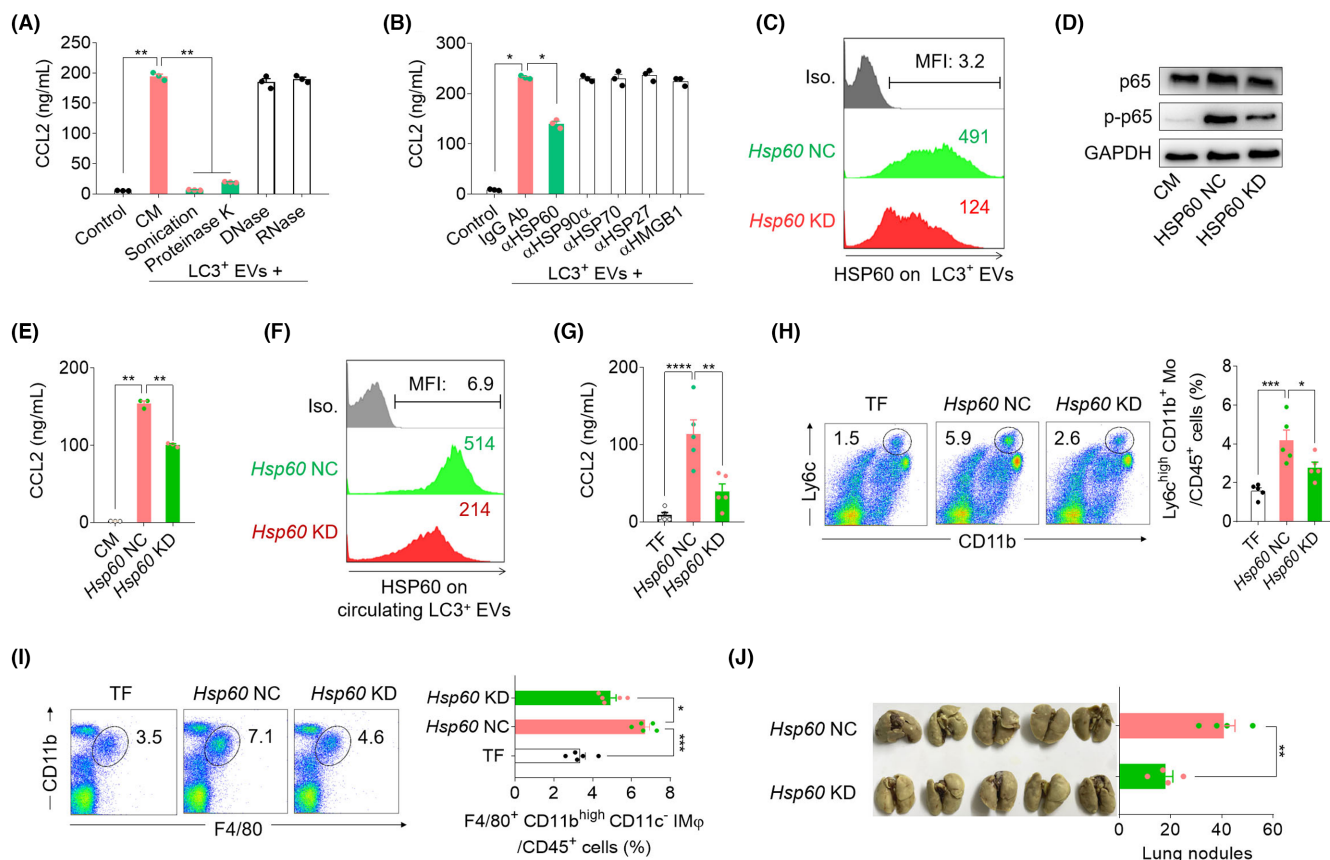
FIGURE 4 HSP60 on intact LC3+ extracellular vesicles (EVs) is essential for CCL2 induction. (A, B,) ELISA detection of CCL2 secretion by lung fibroblasts treated with indicated LC3+ EVs (A) or blocking antibody-pretreated LC3+ EVs for 48 h (B). (C), Flow cytometry (FCM) determination of HSP60 expression on 4T1-LC3+ EVs from *Hsp60* NC- and *Hsp60* KD-4T1 cells. (D), Western blot analyses of the phosphorylation of p65 in lung fibroblasts treated with *Hsp60* NC- or *Hsp60* KD-4T1-LC3+ EVs for 30 min. (E), ELISA detection of CCL2 secretion by lung fibroblasts treated with *Hsp60* NC- or *Hsp60* KD-4T1-LC3+ EVs for 48 h. F-J, BALB/c mice (*n* = 5) were s.c. injected with *Hsp60* NC- or *Hsp60* KD-4T1 cells. On day 10, the peripheral blood was collected and HSP60 expression on cLC3+ EVs was determined by FCM (F). CCL2 levels in supernatants from the lung fibroblasts were tested by ELISA (G). The proportion of monocytes (Mo) (H) and interstitial macrophages (IMφ) (I) in the lung was analyzed by FCM. On day 35, lung metastatic nodules were counted (J). Data were expressed as means ± SEM.

CCL2 is the major driving force for LC3+ EVs–induced inflammatory and immunosuppressive PMN formation in vitro and in vivo.

3.5 | Circulating LC3+ EVs and HSP60 on cLC3+ EVs were associated with disease progression and lung metastasis in patients with BC

We first verified the effect of human BC cell–derived LC3+ EVs (hLC3+ EVs) on human lung fibroblasts. MDA-MB-231–derived hLC3+ EVs induced HFL1 activation (Figure S7B) and CCL2 secretion (Figure 6A, Figure S7A). Blocking of HSP60 partially reduced hLC3+ EVs–induced CCL2 secretion (Figure S7C, Figure 6B), indicating that hLC3+ EVs could significantly stimulate CCL2 production in human lung fibroblasts through HSP60.

To observe the relationship of cLC3+ EVs and HSP60 level with lung metastasis occurrence, the plasmas from BC patients and healthy donors (HDs) (Table S1) were collected for cLC3+ EVs

quantification. The number of cLC3+ EVs in the plasma of BC patients was substantially higher than that in HDs (Figure 6C-E). Higher proportion of cLC3+ EVs from BC patients contained epithelial cell adhesion molecule (EpCAM) compared with HDs (Figure S7D), suggesting a cancer cell origin of most of the cLC3+ EVs from BC patients.[27] Further analysis revealed that the number of LC3+ EVs in the plasma of BC patients was positively correlated with the progression of BC (Figure 6E). Importantly, the number of cLC3+ EVs in BC patients with lung metastasis was significantly higher than that in BC patients without metastasis (Figure 6F). Of note, the number of cLC3+ EVs in the plasma of patients with TNBC was markedly higher than that with non–triple-negative breast cancer (NTNBC) (Figure 6G). Accordingly, the HSP60 level on cLC3+ EVs was also significantly higher in BC patients compared than in HDs (Figure 6H). Among BC patients, the HSP60 level on cLC3+ EVs was significantly higher in patients at stage IV than that in patients at stage I/II and III (Figure 6H); the HSP60 level on cLC3+ EVs in BC patients with lung metastasis was significantly higher than that in BC patients

without metastasis (Figure 6I); and the HSP60 level on cLC3$^+$ EVs was markedly higher in patients with TNBC than in patients with NTNBC (Figure 6J). These results suggest that cLC3$^+$ EV number and HSP60 level on cLC3$^+$ EV in plasma are closely related to disease progression and lung metastasis in BC patients.

Binary logistic regression analysis showed that cLC3$^+$ EV number and HSP60 level on cLC3$^+$ EVs were risk factors for lung metastasis of BC (Tables S3 and S4). ROC curve revealed that the area under the cLC3$^+$ EV curve, the HSP60 curve, and the curve of the combination were 0.898, 0.694, and 0.910, respectively (Figure 6K-M), indicating the synergic impact of combining the two biomarkers. These results suggest that cLC3$^+$ EV number and HSP60 level on cLC3$^+$ EV in the plasma have a potential value as biomarkers for lung metastasis in patients with BC.

4 | DISCUSSION

In summary, we unraveled the novel mechanism of LC3$^+$ EVs–enhanced lung PMN formation of BC as follows (Figure 7): (1) The primary tumor–released LC3$^+$ EVs activate lung fibroblasts to produce CCL2 via the HSP60-TLR2-MyD88-NF-κB pathway; (2) CCL2 could then recruit Mo to the lungs; (3) lung PMN formation characterized by Mo and macrophages infiltration, immunosuppression, and enhanced vascular permeability eventually promotes lung metastasis. Our findings imply that HSP60 on cLC3$^+$ EVs or CCL2 production might be potential targets for the prevention and treatment of lung metastasis in patients with BC; the number of cLC3$^+$ EVs and HSP60 level on cLC3$^+$ EV in the plasma might serve as biomarkers of patients with BC regarding the risk of metastasis.
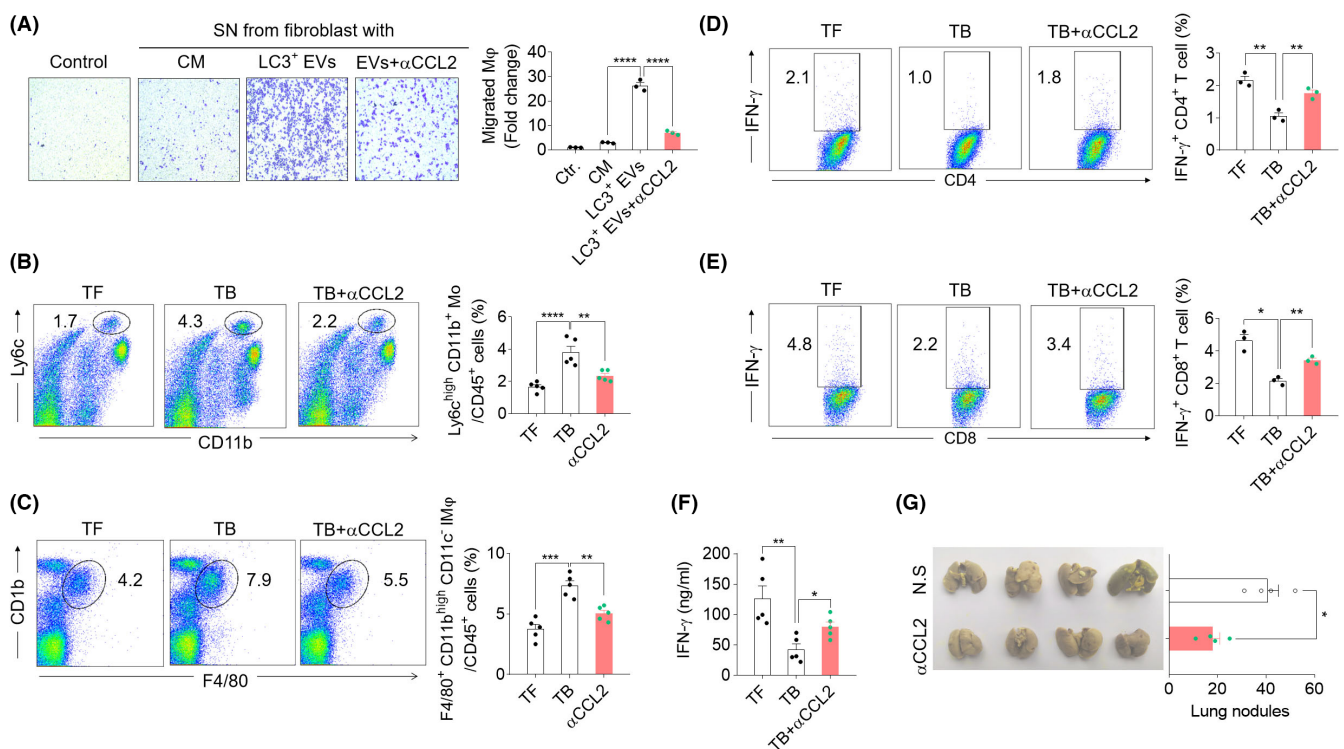

FIGURE 5 CCL2 is responsible for premetastatic niche (PMN) formation and lung metastasis. A, Representative pictures (100×) of Raw264.7 migration toward indicated supernatants. B-G, BALB/c mice ($n = 5$) were s.c. injected with 4T1 cells and then intraperitoneally injected with anti-CCL2 antibody every other day for four times from the second day of tumor inoculation. On day 10, the proportion of monocytes (Mo) (B) and interstitial macrophages (IMφ) (C) from the lung were analyzed by flow cytometry (FCM). The lung infiltrating lymphocytes were stimulated with anti-CD3/CD28 mAb. Intracellular IFN-γ expression of CD4$^+$ T cells (D) and CD8$^+$ T cells (E) was analyzed by FCM, and IFN-γ secretion in supernatants was detected by ELISA (F). On day 35, lung metastatic nodules were analyzed (G). Data were expressed as means ± SEM.

FIGURE 6 Detection of circulating LC3$^+$ extracellular vesicles (EVs) in the plasma of breast cancer (BC) patients is associated with diagnosis of lung metastasis. A, B, ELISA detection of CCL2 secretion by HFL1 treated with LC3$^+$ EVs for 48 h (A) and with anti-HSP60 mAb pretreatment (B). C, D, Flow cytometry (FCM) pictures of cLC3$^+$ EV number (C) and HSP60 level on cLC3$^+$ EVs (D) in plasma of HDs and BC patients. E-G, cLC3$^+$ EV number of HDs ($n = 30$) and BC patients with different stages ($n = 104$) (E), BC patients with non-metastasis ($n = 75$) or lung metastasis ($n = 29$) (F), BC patients with non–triple-negative breast cancer (NTNBC) ($n = 53$) or triple-negative breast cancer (TNBC) ($n = 29$) (G). H-J, HSP60 MFI on cLC3$^+$ EVs of healthy donors (HDs) and BC patients with different stages (H), BC patients with nonmetastasis or lung metastasis (I), BC patients with TNBC or NTNBC (J). (K–M) The ROC curve of cLC3$^+$ EVs (K), HSP60 (L), and cLC3$^+$ EVs combined with HSP60 (cLC3$^+$ EVs + HSP60) (M). Data were expressed as means ± SEM.
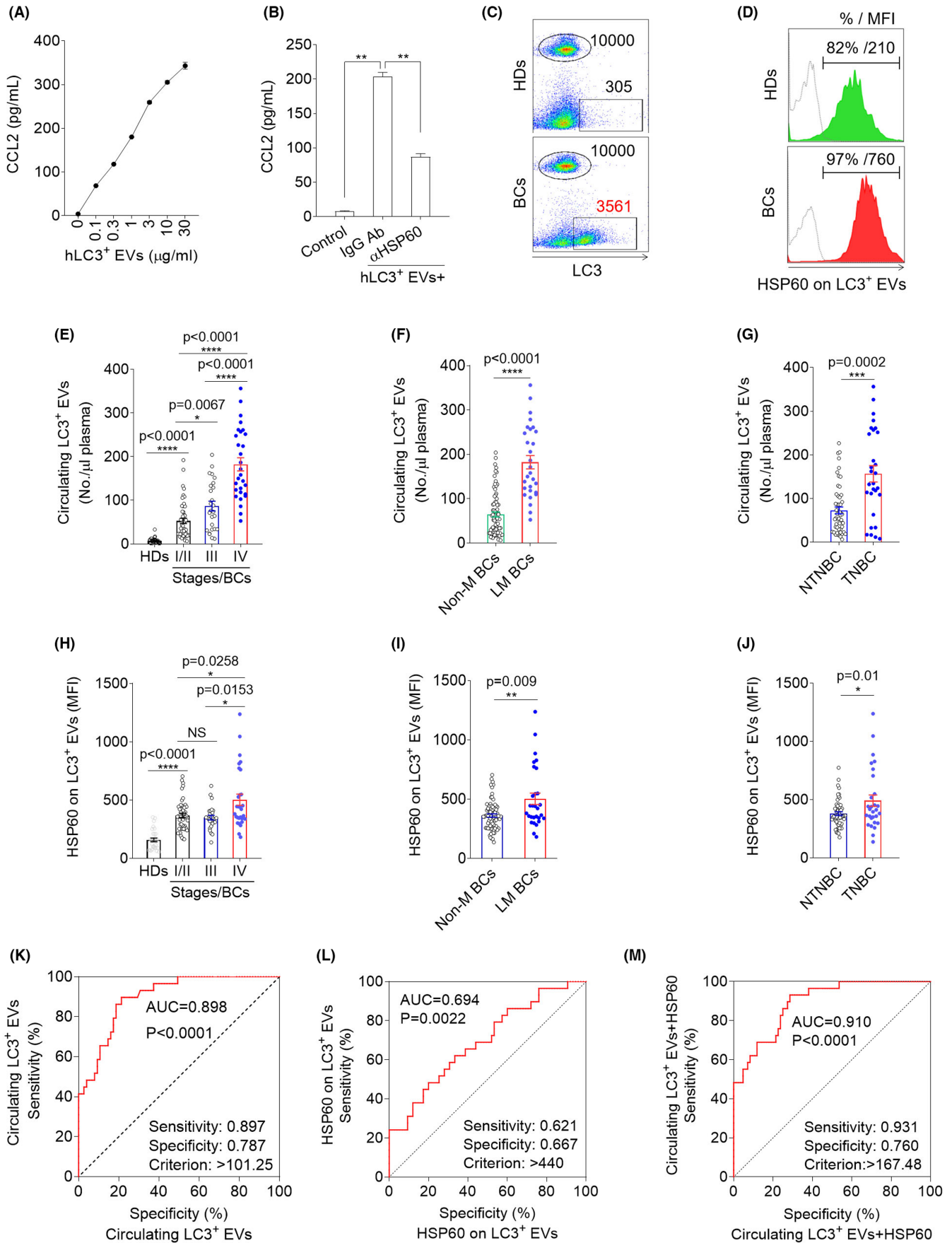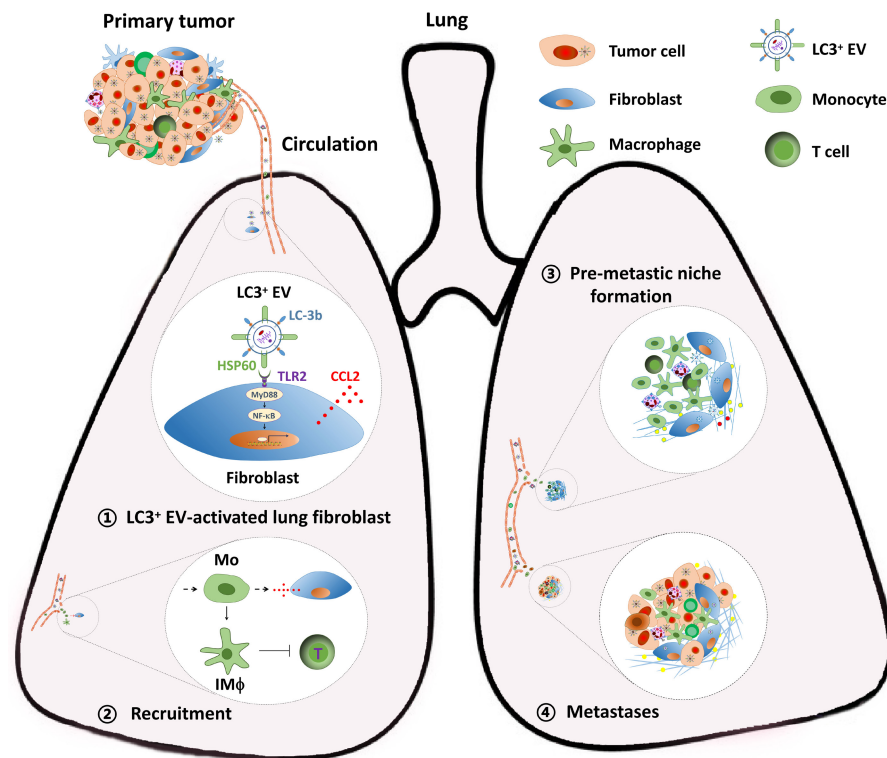
FIGURE 7 Schematic illustration of circulating LC3+ extracellular vesicles (EVs) that promote lung premetastatic niche (PMN) formation and metastasis by educating fibroblast.

4.1 | Tumor cell–released LC3+ EVs as a new TDSF

The formation of PMN involves crosstalk among various primary TDSFs, the host stromal microenvironment, and mobilized BMDCs within future metastatic sites.[7] Primary tumor-derived EVs, such as exosomes which contain proteins, mRNA, or microRNA, could travel far from their original site to act as potential mediators for educating the PMN.[28–30] In the present study, extracellular secretory autophagosomes carrying the autophagosomal marker LC3II, but not exosomal markers CD63 or TSG101, with sizes ranging from 200 to 900nm as previously identified,[19,20] play the crucial role in promoting an inflammatory and immune-suppressive lung PMN and subsequently enhance metastasis.

4.2 | Effect of fibroblast-derived CCL2 on PMN

CCL2 is known to be involved in the pathogenesis of several diseases characterized by monocytic infiltration.[31,32] Evidence suggests that cancer-associated fibroblasts–derived CCL2 can recruit a variety of myeloid cells including TAM and inflammatory Mo, promoting tumor inflammatory microenvironment formation and metastasis.[33,34] Furthermore, tumor or stroma-derived CCL2 can recruit inflammatory Mo, promoting tumor metastasis.[35] In this study, RNA sequencing revealed high expression of inflammatory cytokines, such as CCL2 and IL-6, in lung fibroblasts upon cLC3+ EVs stimulation. To explore the mechanistic role of CCL2 in lung metastasis, CCL2 antibody was injected in vivo. As expected, Mo and macrophages were decreased, T cell function was recovered, lung PMN characteristics were weakened, and lung metastasis was decreased in mice treated

with CCL2 antibody. These data illustrate the mechanistic role of CCL2 in the pathogenesis of lung metastasis.

Fibroblasts have been proved to be involved in the progression of PMN and metastasis. Therefore, we focus on lung fibroblasts in this study. However, other cell subsets in the lungs may also take up LC3+ EVs and play roles in PMN formation. Recent studies have demonstrated that tumor-derived exosomes could polarize macrophages toward an immunosuppressive phenotype characterized by increased PD-L1 expression.[36] Furthermore, the tumor cell–released microparticles were reported to remodel the lung parenchyma via a macrophage-dependent pathway to create an altered inflammatory and mechanical response to tumor cell invasion.[37] We also found that LC3+ EVs could be taken up by macrophages in the lungs (Figure 3B). In view of the above, macrophages may also be involved in LC3+ EVs–promoted PMN formation. The role of macrophages in this process awaits to be explored in the future.

4.3 | PD-L1 upregulation in lung Mo and IMs upon LC3+ EVs injection could contribute to immunosuppression in PMN

Our previous report showed that in tumor microenvironment, tumor-derived autophagosomes (LC3+ EVs) could convert macrophages into an immunosuppressive M2-like phenotype characterized by the expression of PD-L1 and IL-10. These macrophages inhibited the proliferation of both CD4+ and CD8+ T cells in vitro and promoted tumor growth mainly through PD-L1 in vivo. This mechanism may also be applicable to immunosuppression in PMN. Recent study showed that tumor-derived exosomes modulate PD-L1

expression in Mo, which contributes to cancer-related inflammation and concurrent immune escape via PD-L1 expression in chronic lymphocytic leukemia.[38] Furthermore, tumor-derived exosomes have increased expression of PD-L1 on resident IMφ and subsequently curtail immune responses through inhibition of effector T cell functions and contribute to macrophage-mediated PMN formation.[36] The above research indicated that PD-L1 upregulation in lung IMs or Mo upon tumor-derived EV injection plays an important role in immunosuppression in PMN. In addition, we found that LC3+ EV upregulated PD-L1 on the surface of macrophages by activating IL-6 in fibroblasts in the distal lung tissue in our model (data not shown), which may be another mechanism leading to the inhibition of T cell function and thus promoting the formation of PMN.

4.4 | Circulating LC3+ EV number and membrane-bound HSP60 as potential biomarkers of lung metastasis

Membrane-bound HSP60 on tumor-derived EVs, such as exosomal HSP60, has been reported capable of binding a variety of receptors present on the surface of cells, such as TLRs, and has the potential to be used as a biomarker for the diagnosis in a variety of cancers.[39,40] In line with this finding, our study showed that membrane-bound HSP60 on cLC3+ EVs was crucial in lung fibroblast stimulation by binding TLR2. Moreover, cLC3+ EV number in plasma and HSP60 level on cLC3+ EVs were associated with progression and lung metastasis in BC patients. Notably, due to their bigger size (200-900nm vs 40-100nm for exosomes), LC3+ EVs could be easily quantified by FCM. Thus, from the view of technical convenience, the number of cLC3+ EVs and HSP60 level on cLC3+ EV in the plasma are suitable biomarkers in clinical application. Future clinical studies are warranted to investigate if these two biomarkers could be used to predict lung metastasis or monitor the therapeutic effects in BC patients.

4.5 | Inhibiting HSP60 on cLC3+ EVs might be an alternative antitumor strategy

It has been shown that HSP60 is mostly released by tumor cells but not by normal cells.[41] Consistently, we found abundant amount of HSP60 in LC3+ EVs released by tumor cells, so that the presence of HSP60 on cLC3+ EVs may reflect tumorigenicity. Moreover, the circulating feature of cLC3+EVs might readily explain their tumorigenicity role throughout the body. It has been proved that CCL2 promotes tumor progression mainly by inducing proliferation and migration of tumor cells[42] and recruitment of Mo and MDSCs.[32,33] Although the roles of CCL2 in cancer progression have been understood gradually, drugs modulating the CCL2-CCR2 axis as anticancer agents are clinically not available except for administration in clinical trials. The CCL2-CCR2 axis functions physiologically in various organs such as the lungs and digestive tract, where a variety of immune cells accumulate, so that direct blockade of the CCL2-CCR2

axis potentially causes unexpected effects. Our study revealed that inhibiting HSP60 could partially attenuate CCL2 secretion, indicating that inhibiting HSP60 on cLC3+ EVs might be an alternative antitumor strategy through reducing CCL2 production.

DISCLOSURE

The authors declare no conflict of interest.

ETHICS STATEMENT

This study involves human participants and was approved by the Ethics Committee for Human Studies of Southeast University (2021ZDKYSB026). All participants were given details of the study design and provided signed informed consent. Animal operations were performed according to the National Institutes of Health guidelines. All animal experiments were approved by the Institutional Animal Care and Welfare Committee of Southeast University and strictly followed the animal welfare guidelines of the Institutional Animal Care and Welfare Committee of Southeast University (No. 20200101016). Registry and the Registration No. of the study/trial: N/A.

ORCID

Fang Huang https://orcid.org/0000-0002-6136-8867
Lixin Wang https://orcid.org/0000-0002-3480-4491

REFERENCES

1. Harbeck N, Penault-Llorca F, Cortes J, et al. Breast cancer. *Nat Rev Dis Prim*. 2019;5:1-31.
2. Lambert AW, Pattabiraman DR, Weinberg RA. Emerging biological principles of metastasis. *Cell*. 2017;168:670-691.
3. Bray F, Ferlay J, Soerjomataram I, Siegel R, Torre LA, Jemal A. Global cancer statistics 2018: GLOBOCAN estimates of incidence and mortality worldwide for 36 cancers in 185 countries. *CA Cancer J Clin*. 2018;68:394-424.
4. Peinado H, Zhang H, Matei IR, et al. Premetastatic niches: organ-specific homes for metastases. *Nat Rev Cancer*. 2017;17:302-317.
5. Sleeman JP. The metastatic niche and stromal progression. *Cancer Metastasis Rev*. 2012;31:429-440.
6. Chin AR, Wang SE. Cancer tills the premetastatic field: mechanistic basis and clinical implications. *Clin Cancer Res*. 2016;22:3725-3733.
7. Liu Y, Cao XT. Characteristics and significance of the pre-metastatic niche. *Cancer Cell*. 2016;30:668-681.
8. Kaplan RN, Riba RD, Zacharoulis S, et al. VEGFR1-positive haematopoietic bone marrow progenitors initiate the pre-metastatic niche. *Nature*. 2005;438:820-827.

9. Hiratsuka S, Watanabe A, Sakurai Y, et al. The S100A8-serum amyloid A3-TLR4 paracrine cascade establishes a pre-metastatic phase. *Nat Cell Biol.* 2008;10:1349-1355.

10. Sharon Y, Raz Y, Cohen N, et al. Tumor-derived osteopontin reprograms normal mammary fibroblasts to promote inflammation and tumor growth in breast cancer. *Cancer Res.* 2015;75:963-973.

11. Tang Y, Lu Y, Chen Y, et al. Pre-metastatic niche triggers SDF-1/CXCR4 axis and promotes organ colonisation by hepatocellular circulating tumour cells via downregulation of Prrx1. *J Exp Clin Can Res.* 2019;38:473.

12. Yang C, Wang Z, Li L, et al. Aged neutrophils form mitochondria-dependent vital NETs to promote breast cancer lung metastasis. *J Immunother Cancer.* 2021;9:e002875.

13. Wu X, Zhou Z, Xu S, et al. Extracellular vesicle packaged LMP1-activated fibroblasts promote tumor progression via autophagy and stroma-tumor metabolism coupling. *Cancer Lett.* 2020;478:93-106.

14. Sceneay J, Chow MT, Chen A, et al. Primary tumor hypoxia recruits CD11b+/Ly6Cmed/Ly6G+ immune suppressor cells and compromises NK cell cytotoxicity in the premetastatic niche. *Cancer Res.* 2012;72:3906-3911.

15. Bel S, Pendse M, Wang Y, et al. Paneth cells secrete lysozyme via secretory autophagy during bacterial infection of the intestine. *Science.* 2017;357:1047-1052.

16. Nicolás-Ávila JA, Lechuga-Vieco AV, Esteban-Martínez L, et al. A network of macrophages supports mitochondrial homeostasis in the heart. *Cell.* 2020;183:94-109.

17. Zhou M, Wen Z, Cheng F, et al. Tumor-released autophagosomes induce IL-10-producing B cells with suppressive activity on T lymphocytes via TLR2-MyD88-NF-κB signal pathway. *Onco Targets Ther.* 2016;5:e1180485.

18. Gao R, Ma J, Wen Z, et al. Tumor cell-released autophagosomes (TRAP) enhance apoptosis and immunosuppressive functions of neutrophils. *Onco Targets Ther.* 2018;7:e1438108.

19. Wen ZF, Liu H, Gao R, et al. Tumor cell-released autophagosomes (TRAPs) promote immunosuppression through induction of M2-like macrophages with increased expression of PD-L1. *J Immunother Cancer.* 2018;6:151.

20. Chen YQ, Li PC, Pan N, et al. Tumor-released autophagosomes induces CD4+ T cell-mediated immunosuppression via a TLR2-IL-6 cascade. *J Immunother Cancer.* 2019;7:178.

21. Li Y, Wang LX, Yang G, Hao F, Urba WJ, Hu HM. Efficient cross-presentation depends on autophagy in tumor cells. *Cancer Res.* 2008;68:6889-6895.

22. Liu Y, Gu Y, Han Y, et al. Tumor Exosomal RNAs promote lung pre-metastatic niche formation by activating alveolar epithelial TLR3 to recruit neutrophils. *Cancer Cell.* 2016;30:243-256.

23. Kowanetz M, Wu X, Lee J, et al. Granulocyte-colony stimulating factor promotes lung metastasis through mobilization of Ly6G+Ly6C+ granulocytes. *Proc Natl Acad Sci USA.* 2010;107:21248-21255.

24. Kuzet SE, Gaggioli C. Fibroblast activation in cancer: when seed fertilizes soil. *Cell Tissue Res.* 2016;365:607-619.

25. Ji Q, Zhou L, Sui H, et al. Primary tumors release ITGBL1-rich extracellular vesicles to promote distal metastatic tumor growth through fibroblast-niche formation. *Nat Commun.* 2020;11:1211.

26. Wang L, Cao L, Wang H, et al. Cancer-associated fibroblasts enhance metastatic potential of lung cancer cells through IL-6/STAT3 signaling pathway. *Oncotarget.* 2017;8:76116-76128.

27. Gires O, Pan M, Schinke H, Canis M, Baeuerle PA. Expression and function of epithelial cell adhesion molecule EpCAM: where are we after 40 years? *Cancer Metastasis Rev.* 2020;39:969-987.

28. Liu Y, Gu Y, Cao X. The exosomes in tumor immunity. *Oncoimmunology.* 2015;4:e1027472.

29. Costa-Silva B, Aiello NM, Ocean AJ, et al. Pancreatic cancer exosomes initiate pre-metastatic niche formation in the liver. *Nat Cell Biol.* 2015;17:816-826.

30. Costa-Silva B, Aiello NM, Ocean AJ, et al. Primary prostate cancer educates bone stroma through exosomal pyruvate kinase M2 to promote bone metastasis. *J Exp Med.* 2019;216:2883-2899.

31. Li X, Yao W, Yuan Y, et al. Targeting of tumour-infiltrating macrophages via CCL2/CCR2 signalling as a therapeutic strategy against hepatocellular carcinoma. *Gut.* 2015;66:157-167.

32. Raghu H, Lepus CM, Wang Q, et al. CCL2/CCR2, but not CCL5/CCR5, mediates monocyte recruitment, inflammation and cartilage destruction in osteoarthritis. *Ann Rheum Dis.* 2017;76:914-922.

33. Yang X, Lin Y, Shi Y, et al. FAP promotes immunosuppression by cancer-associated fibroblasts in the tumor microenvironment via STAT3-CCL2 signaling. *Cancer Res.* 2016;76:4124-4135.

34. Xiang H, Ramil CP, Hai J, et al. Cancer-associated fibroblasts promote immunosuppression by inducing ROS-generating monocytic MDSCs in lung squamous cell carcinoma. *Cancer Immunol Res.* 2020;8:436-450.

35. Qian BZ, Li J, Zhang H, et al. CCL2 recruits inflammatory monocytes to facilitate breast-tumour metastasis. *Nature.* 2011;475:222-225.

36. Morrissey SM, Zhang F, Ding C, et al. Tumor-derived exosomes drive imunosuppressive macrophages in a pre-metastatic niche through glycolytic dominant metabolic reprogramming. *Cell Metab.* 2021;33:2040-2058.

37. Zhang H, Yu Y, Zhou L, et al. Circulating tumor microparticles promote lung metastasis by reprogramming inflammatory and mechanical niches via a macrophage-dependent pathway. *Cancer Immunol Res.* 2018;6:1046-1056.

38. Haderk F, Schulz R, Iskar M, et al. Tumor-derived exosomes modulate PD-L1 expression in monocytes. *Sci Immunol.* 2017;2:eaah5509.

39. Vocka M, Langer D, Fryba V, et al. Novel serum markers HSP60, CHI3L1, and IGFBP-2 in metastatic colorectal cancer. *Oncol Lett.* 2019;18:6284-6292.

40. Zanin-Zhorov A, Cohen IR. Signaling via TLR2 and TLR4 directly Down-regulates T cell effector functions: the regulatory face of danger signals. *Front Immunol.* 2013;4:211.

41. Campanella C, Bucchieri F, Merendino AM, et al. The odyssey of Hsp60 from tumor cells to other destinations includes plasma membrane-associated stages and Golgi and exosomal protein-trafficking modalities. *PLoS One.* 2012;7:e42008.

42. Loberg RD, Ying C, Craig M, Yan L, Snyder LA, Pienta KJ. CCL2 as an important mediator of prostate cancer growth in vivo through the regulation of macrophage infiltration. *Neoplasia.* 2007;9:556-562.

SUPPORTING INFORMATION

Additional supporting information can be found online in the Supporting Information section at the end of this article.